HHS Public Access

Author manuscript

Ultrasound Med Biol. Author manuscript; available in PMC 2021 January 01.

Published in final edited form as:

Ultrasound Med Biol. 2020 January ; 46(1): 122–136. doi:10.1016/j.ultrasmedbio.2019.08.024.

Distribution and Diffusion of Macromolecule Delivery to the Brain via Focused Ultrasound using Magnetic Resonance and Multispectral Fluorescence Imaging

Michael A. Valdez[1], **Elizabeth Fernandez**[1], **Terry Matsunaga**[1,4], **Robert P. Erickson**[2,3], **Theodore P. Trouard**[1,3,4,5,*]

[1]Department of Biomedical Engineering, University of Arizona, Tucson, AZ

[2]Department of Pediatrics, University of Arizona, Tucson, AZ

[3]BIO5 Research Institute, University of Arizona, Tucson, AZ

[4]Department of Medical Imaging, University of Arizona, Tucson, AZ

[5]Evelyn F. McKnight Brain Institute, University of Arizona, Tucson, AZ

Abstract

Focused ultrasound (FUS), in combination with microbubble contrast agents, can be used to transiently open the blood brain barrier (BBB) to allow intravascular agents to cross into the brain. Often, FUS is carried out in conjunction with magnetic resonance imaging (MRI) to evaluate BBB opening to gadolinium-based MRI contrast agents. While MRI allows direct visualization of the distribution of gadolinium-based contrast agents in the brain parenchyma, it does not allow measurements of the distribution of other molecules crossing the BBB. Therapeutic molecules, e.g. monoclonal antibodies, are much different in size than MRI contrast agents and have been shown to have different distributions in the brain following FUS-mediated BBB opening. In this work, we have combined *in vivo* MRI and *ex vivo* multispectral fluorescence imaging to compare the distribution of MRI contrast and dextran molecules of different molecular weights (3, 70 and 500 kDa) following FUS-mediated BBB opening through a range of ultrasound pressures (0.18 – 0.46 MPa) in laboratory mice. The volume of brain exposed was calculated from the MRI and fluorescence images and was significantly dependent on both molecular weight and ultrasound pressure. Diffusion coefficients of the different molecular weight dextran molecules in the brain parenchyma were also calculated from the fluorescence images and were negatively correlated with the MW of the dextran molecules. The results of this work build on a body of knowledge that is critically important for the FUS technique to be used in clinical delivery of therapeutics to the brain.

*To whom correspondence should be addressed.

Keywords

Blood brain barrier; focused ultrasound; microbubbles; magnetic resonance imaging; drug delivery; mice

Introduction

The effectiveness of drugs for treating neurological diseases is hindered by the inability of these agentss to cross the blood-brain barrier (BBB) (Pardridge 2005). The BBB refers to the set of unique endothelial cells that line the vasculature in the brain and effectively controls movement of molecules into and out of the brain. While necessary for proper brain function, the BBB blocks 98% of drugs from entering the brain (Pardridge 2005), and is a significant barrier to the successful development of therapies for neurodegenerative diseases. Unless significant advancements are made to safely deliver drugs to the brain, improved treatments for neurological disease, such as Alzheimer's Disease (AD), will remain limited. A number of techniques have been used to circumvent the BBB, but are often highly invasive and/or ineffective. Intraventricular infusion is a poor method for drug delivery because it requires highly invasive skull penetration and introduces the risk of infection. In addition, drugs are rapidly cleared by the cerebrospinal fluid (CSF) and diffusion of drugs into tissue can be minimal (Pardridge 2011). Chemical disruption of the BBB can cause chronic neuropathologic sequelae and vascular damage (Gabathuler 2010). Active transport allows some specific molecules to cross the BBB (Boado et al. 2010), but therapeutic development using this route has been met with limited success.

Over the last two decades, a minimally invasive technique to transiently open the BBB has been under development that utilizes transcranial focused ultrasound (FUS) in combination with intravascular microbubble (μB) contrast agents. This method is often carried out in conjunction with magnetic resonance imaging (MRI) to guide and assess BBB opening and has been referred to as MRI guided FUS (MRgFUS) (Chen et al. 2013; Choi et al. 2007; Hynynen et al. 2001; Hynynen et al. 2003; Hynynen et al. 2005; Kinoshita et al. 2006a). Opening the BBB in this way allows drugs to enter the interstitial fluid (ISF) (i.e., the extracellular fluid) of the brain parenchyma. ISF is replaced every 20 hours, which is ~5.5 times longer than CSF (Calias et al. 2014). Therefore, MRgFUS would likely improve effectiveness compared to currently used methods to deliver therapeutics to the CSF.

Many MRgFUS studies to date have been carried out in rodents to assess MRgFUS for delivery or therapy in a variety of neurological disorders including cancer, Parkinson's Disease and AD (Burgess and Hynynen 2014; Jordão et al. 2010; Kinoshita et al. 2006a; Kinoshita et al. 2006b; Raymond et al. 2008). MRgFUS has also been carried out in nonhuman primates where the method has been shown to be safe (Boado et al. 2010; Downs et al. 2015; Marquet et al. 2011a; Marquet et al. 2011b). Recently, clinical trials using MRgFUS in humans have been reported for the treatment of Alzheimer's disease (Lipsman et al. 2018).

Microbubbles refer to small perfluorocarbon gas bubbles encapsulated by a lipid shell, and are FDA approved for contrast-enhanced ultrasound for cardiac imaging because they are

safe and reflect ultrasound with high efficiency. For BBB opening, stable or inertial cavitation of the microbubble in the presence of ultrasound is believed to be responsible for eliciting this response (McDannold et al. 2006; Sun et al. 2015; Tung et al. 2010). Cavitation is the rapid shrinking and expansion of the bubble due to the alternating pressure of the ultrasound and the greater compressibility of gas relative to its liquid environment. The cavitation causes mechanical forces around each microbubble in the form of shock waves, microjets, and/or microstreaming. In small vessels of the brain (e.g. capillaries and arterioles), these forces can disrupt the endothelial tight junctions, which effectively disrupts the BBB and allows passage of molecules from the vasculature to the brain parenchyma. Besides disruption of the tight junctions, other mechanisms may contribute to permeabilization of the capillaries, such as the formation of pores in the capillary endothelium (Nhan et al. 2013).

While drug delivery using MRgFUS has been incorporated into clinical trials (Lipsman et al. 2018), preclinical studies in animal models will continue to aid in the translation of this technique into a clinically effective and safe method for enhancing drug delivery to the brain. In this work, we have characterized the distribution of molecules in the brain of mice following MRgFUS procedures at difference pressures. Specifically, the dependence of the molecular weight of the molecule to be delivered to the brain was evaluated under identical MRgFUS settings. Previous work has addressed this question, but necessarily used different mice to study different molecular weight dextrans (Choi et al. 2010). By using multiple fluorescence moieties on different molecular weight dextran, the effect of molecular weight on the diffusion and distribution of molecules in the brain following MRgFUS can be determined in the same mouse under identical conditions. This has allowed direct visualization and comparison of the distribution of different molecular weight detrains and mathematical modeling of dextran diffusion within the brain.

Materials and Methods

Mice

Mice of the C57BL/6J inbred strain of both sexes and of ages greater than 6 weeks were used for these experiments (The Jackson Laboratory, Bar Harbor, ME, USA). They were maintained with ad libitum food and water and experimental protocols were approved by the Institutional Animal Care and Use Committee at the University of Arizona.

Microbubbles

Microbubble solutions were prepared at least one day before use with a mixture of 1,2-dipalmitoyl-sn-glycero-3-phosphocholine (DPPC), 1,2-dipalmitoyl-sn-glycero-3 phosphate (DPPA), and 1,2-dipalmitoyl-sn-glycero-3-phosphoethamolamine-N-polyethyleneglycol)-2000 (DPPE-PEG-2000) (Avanti Polar Lipids, Alabaster, AL, USA). Lipids were dissolved in propylene glycol by heating to approximately 60° C followed by reconstitution with normal saline and glycerol to achieve a final lipid concentration of 1 mg/ml. The resulting opalescent lipid colloids were placed in 2 mL glass vials and sealed. The headspace of the vials was purged with perfluorobutane (Fluoromed, Round Rock, TX, USA) and stored at 4°C until used. Just before use, microbubbles were ‘activated’ by

agitating the sealed vials at 4,500 rpm for 45 seconds using a VIALMIX™ vial shaker (Lantheus Medical Imaging, New York, NY, USA). Sizing was conducted on a Malvern Nano Zetasizer (Malvern Panalytical, Malvern, UK). The microbubbles were approximately 1 micron in size and had a concentration of approximately 1-5 × 10^9 microbubbles per mL (Harpel et al. 2016).

A 1 mL insulin syringe with a 27-gauge needle was loaded with 0.5 ml of sterile saline. The agitated vial was inverted gently several times to resuspend the μBs and five times the μB dose was drawn up into the syringe. The syringe was then gently inverted several times and rotated until the diluted microbubbles appeared fully mixed. 100 μL of the diluted microbubbles were injected into an animal for a final non-diluted dose of 0.2 mL per kg of body weight. This dose is 20x greater than the starting FDA-recommended human dose but 5x less than the maximum dose safely used in murine animal models in preclinical studies (Howles et al. 2010). The microbubbles were injected approximately 15 minutes after activation, and a fresh vial of microbubbles was used for each animal.

Focused Ultrasound

A single-element transducer with a 22 mm diameter, a focal length of 19 mm, and an operating frequency of 2.0 MHz was used in all experiments. The transducer was connected to a custom FUS driver (Synergy Electronics, Scottsdale, AZ, USA) that controlled the timing and pressure of ultrasound pulses. The beam shape and pressure of the FUS transducer and driver was characterized in degassed water using an Onda (Sunnyvale, CA, USA) HGL-0200 hydrophone connected to an AH-2010 preamplifier. The beam profile was approximately Gaussian with axial and radial full-width-half-max values of 4.1 and 1.2 mm, respectively. A cleaned, ex vivo mouse skull was placed in between the transducer and hydrophone to estimate the attenuation of pressure in vivo.

A custom animal platform was designed and manufactured that supported the mouse in a supine position at the correct height above the transducer such that the center of the focus of the transducer was within the brain of the mouse (Figure 1). The platform also provides anesthesia to the mouse while it is on the platform. The acoustic window of the platform was shaped to the crown of the mouse head, so that when the mouse was properly placed on the platform, the scalp of the mouse was in contact with the water directly above the FUS transducer. An adjustable nose cone was designed into the platform to deliver anesthesia and was angled downward to help immobilize the head. The entire apparatus is placed into a tank of degassed water (not shown) such that the water comes up to the base of the platform and the scalp of the mouse is just under water. Mice undergoing FUS were first anesthetized with 1.5% isoflurane in a gas chamber. Once under anesthesia, mice were transferred to a heated work surface and a nose cone was used to continue delivery of anesthesia. The scalp fur was removed with scissors followed by CVS depilatory cream (CVS, Woonsocket, RI, USA). Microbubbles, prepared ahead as described above, were injected into the lateral tail vein slowly with gentle pressure applied to the syringe plunger. The diluted microbubbles in the barrel were monitored during injection to ensure there was no visual change in the appearance that would indicate microbubble collapse, (i.e. the cloudy solution turning clear).

Following the tail vein injection of the microbubble solutions, each mouse was placed in a supine position on the FUS bed with the head centered over the acoustic window. Slight pressure was applied to the jaw to ensure the skull was aligned with the acoustic window in which the scalp was partially submerged in water. Anesthesia was directed to the nose cone and it was positioned over the jaw to stabilize the head with slight pressure against the jaw. Within 30 s after microbubble injection, the FUS was turned on for two minutes (10 ms pulses at 1% duty cycle). FUS was targeted to the anterior region of the right parietal bone and traversed the somatomotor area of the isocortex and the caudate putamen. This location was selected for the clinical relevance to neurological diseases and to minimize the amount of tissue borders in the FUS focus region. Targeting was carried out based on prior experiments that characterized the focal region of the transducer with respect to the acoustic window in the positioning apparatus (Figure 1). A visual inspection of the water surface distortion ensured that the FUS was pulsing at the expected location within the acoustic window. Adjustments to the transducer focus location were made as necessary by adjusting the translation stages via the micrometer drive adjustment knobs.

To align the focus in the mouse brains, several mice were used for alignment calibration (data not shown). Mice were anesthetized and placed on the animal holder with the head within the FUS window. Following BBB opening with a derated peak ultrasound pressure of 0.420 MPa, T1-weighted MRI was performed as described below. Vertical (z-axis) adjustment of the ultrasound focus was validated to be appropriate and the x-y displacement from the center of the opened BBB region to the center of the desired brain target was measured on a transverse, aka horizontal, MRI image. For final calibration, the x-y translation stages of the FUS apparatus were adjusted accordingly to move the FUS focus to the desired brain target. Reproduction of the position of the mice within the acoustic window was necessary to reproduce the region of BBB opening.

Magnetic Resonance Imaging

Immediately following the application of FUS, mice received Gd-based MRI contrast agent (Gadobenate dimeglumine; MultiHance; Gd-BOPTA; Bracco Diagnostics Inc., Monroe Township, NJ, USA) introduced via an intraperitoneal injection at 0.1 mmol/kg of body weight (or 6.4 mL/kg). Mice were placed in a heated MRI mouse cradle and were secured with ear and bite bars. A built-in nose cone was used to deliver anesthesia. Body temperature was monitored via a fiber optic rectal temperature probe and respiration was monitored with a sealed pillow place underneath the animal and connected to a pressure transducer (SA Instruments, Inc., Stony Brook, NY, USA). The MRI cradle slid into the bore of a Bruker BioSpec 7T MRI system (Bruker Medical, Boston, MA, USA) for imaging. A 72 mm Bruker linear volume birdcage coil was used for RF transmission and a 4-channel mouse head phased array coil was used for reception. Horizontal, sagittal, and coronal T1-weighted spin-echo images were obtained using the following parameters: TR/TE = 400/9 ms, FOV = 1.92 × 1.92, matrix size = 128×128, slice thickness = 750 um. In some animals, co-localized T2-weighted images were obtained with a fast spin-echo pulse sequence to evaluate the presence of edema from BBB damage. Imaging parameters were TR/TEeff = 6000/56 ms, echo train length = 8, echo spacing = 14 ms, FOV = 1.92 × 1.92, matrix size = 128×128, slice thickness = 750 um. MRI required approximately 20 minutes. MRI experiments were

carried out at different ultrasound pressures to evaluate the BBB opening prior to the administration of labeled dextran molecules. The results of these experiments were used to establish the parameters (FUS pressures) used in the dextran experiments.

Fluorescent Dextran

Dextran molecules (Thermo Fisher Scientific, Waltham, MA, USA) of 3 different molecular weights (3, 70 and 500 kDa), labeled with three different fluorescent moieties (Cascade Blue, Texas Red and Fluorescein, respectively) were used in the experiments. Dextrans were labeled based on the number of dextran subunits (degree of labeling), such that 1 mg of dextran of any molecular weight (MW) should quantitatively have the same fluorescence. Importantly, dextrans were lysine-fixable, meaning they could be fixed in place (crosslinked with proteins) using formalin or paraformaldehyde (PFA) without washout of the dextrans from the brain. The molecular weight, fluorescent moiety name, absorption/emission wavelength and emission “color” are listed in Table 1. One mg of each dextran was combined and dissolved in 100 μL of PBS, and was injected IV into the tail vein immediately following MRI validation of BBB opening while the mouse was still anesthetized. The dextran was allowed to circulate for 20 minutes, after which transcardial perfusion for fixation of tissues was performed.

Brain Perfusion and Tissue Preparation—While remaining under anesthesia (increased to 2.5% isoflurane in oxygen) mice were perfused with 30 mL of 4% PFA as previously described (Gage et al. 2012). Following perfusion, mouse heads were removed and placed in 10 mL of 4% PFA for 24 hours at 4°C. The brains were then removed from the skull and placed in 4% PFA for 24 hours, followed by cryoprotection in 15% sucrose for 24 hours and 30% sucrose for 24 hours. For fluorescence microscopy, following cryoprotection, brains were imbedded in Tissue-Tek OCT compound (Sakura Finetek, Leiden, The Netherlands) in cryomolds and snap-frozen in isopentane chilled with a slurry of dry ice pellets and ethanol. Frozen brains were wrapped in foil, sealed in an airtight plastic bag, then stored at −80°C freezer until sectioning. Brains were transported on dry ice to a Microm™ HM550 Cryostat microtome (Thermo Scientific, Kalamazoo, MI, USA) for sectioning. The cryostat temperature setting for the specimen was −12 °C and −15 °C for the chamber. The temperature was decreased if the tissue was too soft or increased if too brittle. Coronal sections were cut at a thickness of 100 microns with a cutting angle of 7 degrees. Sections were allowed to thaw on room-temperature slides and then re-frozen on dry ice. The slides were stored at −80°C until imaged

Some mice that underwent FUS mediated BBB opening were used to evaluate tissue damage from the FUS procedure. These “MRI-only” mice did not get an injection of fluorescent dextran, but were perfused immediately after MRI-validated BBB opening, as described above. Procedures and results specific to these mice are included in the Supplemental Material.

Fluorescence Microscopy—Frozen brain sections were imaged with an Olympus MVX10 MacroView fluorescence stereoscope (1x objective lens) which is capable of a resolution up to 1500 lines/mm, a FOV of 55 mm, and magnification from 4x to 125x

(Olympus Life Sciences, Waltham, MA, USA). Filter sets for Cascade blue, rhodamine, and fluorescein filter sets were installed into a filter cube, giving the stereoscope the ability to quickly use different filter sets. The mercury lamp was allowed to warm up for one hour prior to experiments to reach thermal stability, and the sections were imaged with all 3 filter sets with an 11 mm field of view and 13.8 micron × 13.8 micron pixel resolution. ImageX CCD and nanoTGI image acquisition software (Photonic Research Systems Ltd., Newhaven, UK) was used to control the camera and capture the fluorescent images. Exposure times were 3, 2, and 0.3 seconds for the cascade blue, rhodamine, and fluorescein filter sets, respectively. Exposure times were selected to maximize signal without saturating the camera detector. Background images (with only the black stage plate) were also obtained in order to subtract the background fluorescence from the section images.

Quantification—The primary goal of quantification was to determine the amount of dextran as a function of molecular weight entering the brain following FUS-medicated BBB opening. A secondary aim was to evaluate the relative spatial distribution of each size dextran. Quantification methods were adapted from previously published work (Chen et al. 2013) and are further described subsequently. Using in-house software (MATLAB R2014b, MathWorks, Inc., Natick, MA), a region of interest (ROI) at least 100 pixels in extent manually drawn on the fluorescent images within the contralateral caudoputamen (left, nonsonicated) hemisphere of the brain. The intensity in this region should reflect non-specific binding and background fluorescence signal not related to the BBB opening. Images were then set at a threshold of 3 standard deviations above the mean pixel intensity of the background ROI. Special care was taken during the outlining of the background region so sectioning and perfusion artifacts were not included.

After thresholding, the entire left and right hemispheres were individually and manually outlined. The thresholded pixels within the outlined regions were used to calculate the volume of tissue in the brain exhibiting fluorescence for all sections. The volume of tissue exhibiting fluorescence in the left, i.e. unsonicated, hemisphere was subtracted from the volume on the right (i.e. sonicated) hemisphere to yield the volume of tissue affected by the FUS-mediated BBB opening. The mean fluorescence volume for each group of mice with the same experimental parameters was calculated.

The volume of the brain exposed to Gd-BOPTA was determined from MRI signal enhancement. The signal of the brain intensity was linearly normalized (dorsal to ventral) across each section using in house MATLAB code to compensate for signal drop-off from the sensitivity inhomogeneity of the phased-array surface coil. MRI images were then set at a threshold to 3 standard deviations above the mean pixel intensity of the background ROI. Special care was taken during the outlining of the region so that the ventricles were not included. After thresholding, the entire left and right hemispheres were individually and manually outlined. The thresholded pixels within the outlined regions were used to calculate the volume of tissue in the brain exhibiting signal enhancement. The volume of tissue exhibiting signal enhancement in the left. i.e. unsonicated, hemisphere was subtracted from the volume on the right, i.e. sonicated, hemisphere to yield the volume of tissue affected by the FUS-mediated BBB opening. The mean volume with signal enhancement for each group of mice with the same experimental parameters were then calculated.

To determine the effective diffusion of labeled dextran in the brain following MRgFUS, distribution of dextran molecules after 20 minutes was modeled as isotropic diffusion from continuously supplied points sources. This assumes that the concentration of dextran in the blood remains constant over 20 minutes, that the BBB is only open at specific locations, i.e. not every length of every capillary in the tissue is being opened, but that BBB opening is restricted to certain vascular locations. The justification and limitations of these assumptions are addressed in the discussion section of this paper. A more thorough description of the modeling is provided in the Appendix.

Statistical Analysis—To determine the effect of molecular weight and pressure on the volume of brain tissue exposed to the Gd-BOPTA or dextran, an unpaired 2-tailed Student's t-test between individual groups were performed in Excel.

Results

To determine the pressure at which BBB opening occurs, experiments were carried out using derated (McDannold et al. 2008) peak negative FUS pressures of 0.11, 0.18, 0.26, 0.42, and 0.87 MPa. These correspond to mechanical indices of 0.08, 0.13, 0.19, 0.30 and 0.62, respectively. According to literature (Baseri et al. 2010; Chu et al. 2016; O'Reilly and Hynynen 2012), the lowest pressure (0.11 MPa) was not expected to open the BBB. The highest pressure, 0.87 MPa, is considered to be safe for ultrasound imaging and was included as a positive control for evaluating bioeffects of BBB opening. BBB opening to Gd-BOPTA was quantified from MRI images using the NIH ImageJ software. In all brains, a circular region large enough to surround the largest regions with BBB opening was manually placed over the enhancing region of the brain and the contralateral side of the brain. Signal enhancement was quantified as the ratio of the mean signal in the region of BBB opening to the mean signal from the contralateral side.

FUS pressures of 0.26, 0.42 and 0.87 MPa clearly opened the BBB as seen on the T1-weighted MRI images in Figure 2. At a pressure of 0.18 MPa, there was still visible signal enhancement, but it was much decreased in intensity. At 0.11 MPa, there did not appear to be a significant difference compared to the controls (no FUS, not shown). Thermal bioeffects in these experiments were expected to be minimal. Previous studies (Choi et al. 2007) found that at 20% duty cycle, temperature increase was only 0.5 °C over 30 seconds using 0.67 and 0.80 MPa (0.54 and 0.65 MI, respectively, at 1.525 MHz). With far lower duty cycle, our experiments were not expected to cause thermal bioeffects.

Histology revealed that at 0.87 MPa (0.62 MI) all mice had major or minor damage, and at 0.42 MPa (0.30 MI), mice had only minor damage (See Figure A1). Lower pressures 0.26 MPa (0.18 MI) and 0.18 MPa (0.13 MI) had no visible damage. Control mice were used to ensure that FUS without microbubbles did not cause any damage, and that any signs of damage in brains without FUS were indicative of tissue preparation artifacts. In summary, BBB opening with 0.26 MPa opened the BBB without visible damage. BBB could be further opened with greater pressure (0.42 MPa), while introducing only minor damage. From these results, the decision was made to investigate three different FUS pressures in subsequent experiments: 0.18, 0.26 and 0.42 MPa.

Representative coronal MRI and corresponding fluorescence brain images from mice that underwent FUS are shown in Figure 3 and demonstrate a variety of MRI and fluorescence features. At a pressure 0.42 MPa, MRI signal enhancement from BBB opening to 1.1 kDa Gd-BOPTA shows a diffuse columnar pattern of enhancement, extending from the top of the brain to its base (Figure 3A, B). This is consistent with the broad focus of the single-element transducer, measured in pure water to have full-width-half maximums (FWHM's) of 4.1 mm and 1.2 mm in the axial and radial dimensions, respectively. A similar columnar pattern is seen in the fluorescence images (Figure 3C-E). The blue channel fluorescence image of the 3 kDa dextran from approximately the same coronal section, shows a similar diffuse columnar pattern of enhancement, combined with additional punctate intensities. The red channel image (70 kDa dextran) exhibits a similar distribution within the brain, but less diffuse intensity and more intensity of the punctate spots. The green channel (500 kDa dextran) exhibits primarily punctate spots of intensity, still in a columnar pattern. These images demonstrate that at a pressure of 0.42 MPa the BBB is permeable to molecules up to 500 kDa MW, with the smaller MW molecules able to diffuse from the regions of BBB opening. Fluorescence images with the intermediate FUS pressure of 0.26 MPa (Figure 3F-J) show a slightly different pattern, where the MRI intensity, blue and red fluorescence appear similar to those obtained at higher pressure. However, the green fluorescence image, corresponding to the 500 kDa dextran (Figure 3J) exhibits little fluorescence from dextran. The apparent reduction in vertical extent in the blue and red fluorescence images may indicate a smaller focal zone that meets the BBB opening threshold. MRI and fluorescence images of animal exposed to the lowest FUS pressure, 0.18 MPa (Figure 3K-P), show much less BBB opening at this pressure. Signal enhancement can be seen in the MRI images (Figure 3K,L), but is restricted to a much smaller brain region. The blue channel has a reduced region of diffuse intensity and the red channel only shows a small region of punctate spots. The green channel shows essentially no increase in intensity over background. The focal zone "shortening" effect is more dramatic at the low ultrasound pressure (Figure 3K,L) which also seems to exclude all but the slightest amount of 500 kDa from the extravascular space (Figure 3P). Due to the presence of autofluorescence artifacts in these sections, the fluorescent signal cannot be clearly distinguished as in the other slices (3B-D, 3F-H) even though the signal seems to be elevated in entire caudate putamen.

The volume of brain exposed to MRI contrast agent and fluorescent dextran was quantified and plotted in Figure 4. At the highest pressure (0.42 MPa), the smaller molecules not only cross the BBB, but diffuse easily into the brain, increasing the amount of brain tissue exposed to the contrast. As the molecular weight, and therefore the effective size of the molecule increases, the volume of brain containing MRI contrast and dextran decreases, As the pressure of FUS is decreased, the amount of brain exposed to contrast is decreased, while the relationship between different molecular weights remain the same. Negligible intensity is seen in the controls, where only small amounts of autofluorescence of brain tissue were detected. To be objective, when processing this data, whole-hemispheres were included as regions of interest which contained non-zero levels of autofluorescence which limits the precision of our technique when very little signal from fluorescent dextran is present.

To compare the effects of pressure, the same data was sorted by molecular size as is shown in Figure 5. It is clear that higher FUS pressure increases the amount of tissue exposed to small molecules (i.e. 1.1 kDa GBCA and 3 kDa dextran). Although minimizing the pressure should be safer, the reduced pressure also reduces the amount of brain volume exposed to the small molecules. However, this effect is diminished when using larger molecules, i.e. 70 kDa . In this case, higher FUS pressure does not necessarily deliver large molecules to larger volumes of the brain. In the largest molecule studied, i.e. 500 kDa dextran, there is no significant increase in intensity over controls.

Because the fluorescence images are inherently registered with each other, they can be used in conjunction with a mathematical model of diffusion to estimate the diffusion of dextran in the brain. The mathematical model predicts an effective diffusion coefficient of dextran (D*) from the fluorescence images. The diffusion coefficients of dextran in the brain estimated from the model (see Appendix) are plotted on a log scale versus the estimated hydrodynamic diameters of dextran molecules in Figure 6. The current study employed dextran of MWs = 3, 70, and 500 kDa, corresponding to hydrodynamic diameters of 2.3, 10.2, and 30.6 nm, respectively (Marty et al. 2012)(Chen et al. 2013). Data from previously reported studies measuring diffusion of similar macromolecules in the rat brain cortex (Wolak and Thorne 2013) and turtle cerebellum (Xiao et al. 2008) are included for comparison.

Discussion

In the present work, application of extracranial FUS, in combination with intravascular microbubbles, successfully opened the BBB in mice and the distribution of molecular contrast agents was measured using MRI and fluorescence imaging. The results from the current work are consistent with many previous studies which demonstrate that FUS, in combination with IV microbubbles, can be used to temporarily open the BBB in a safe and effective manner (Burgess et al. 2014; Chen and Konofagou 2014; Choi et al. 2007; Hynynen et al. 2001; Samiotaki et al. 2012).

Reliable BBB opening in mice, without macroscopic damage to brain tissue, was achieved using peak FUS pressures between 0.18 and 0.42 MPa. These pressures are in agreement with previous studies in mice, which found safe BBB opening to MRI contrast agent and 3kDa dextran between 0.15 – 0.46 MPa (Baseri et al. 2010). Those previous studies utilized an ultrasound frequency of 1.525 MHz, yielding MI values of between 1.2 and 0.37. In the present work, a 2.0 MHz transducer frequency was utilized, correspond to MI values between 0.13 and 0.30, also in good agreement with the previous study. It is interesting to note that the MI values for safe BBB opening in mice are somewhat below those of 0.46 and 0.37 used in previous studies in rabbits (McDannold et al. 2008) and rats (Marty et al. 2012), respectively. Differences could be the result of several factors, including differences in the thickness of the skull and scalp of the mice compared to larger animals, differences in the application of ultrasound, e.g. duty cycle, pulse duration, total sonication time, or differences in the characteristics of the microbubbles, e.g. lipid composition, size, concentration, etc.

The amount of contrast agent getting into the brain following BBB opening was highly dependent on the MW of the contrast agent as well as the pressure of FUS being applied. At

fixed FUS parameters, the extravasation of contrast agent into the brain parenchyma decreased with increasing MW. As seen in Figure 4, there was a steep decline in the amount of contrast agent getting into the brain as a function of MW. The trend is most pronounced at 0.42 MPa, and persists at 0.26 MPa. This same trend is apparent at 0.18 MPa, although there is far less fluorescence overall and the decline in the amount of contrast agent is not as significant. These results are consistent with previous FUS experiments in mice which measured the distribution of fluorescein-labeled dextrans of different molecular weights in the brains of mice(Choi et al. 2010). In that work, fluorescently labeled (fluorescein) dextrans of 3, 70 and 2000 kDa were utilized. While increased fluorescence in the brain was observed for 3 kDa and 70 kDa dextran, no increased fluorescence was seen in mice injected with 2000 kDa dextran. he present work extends those results by using different fluorescent labels on different MW dextrans. By doing this, the distribution of different MW dextrans can be studied in individual mice, effectively removing biological and experimental FUS variability between mice and between different MW dextrans. This has resulted in a statistical difference in the amount of brain regions exposed to 3 kDa, versus 70 kDa dextran, a difference that was only a trend in the previous study (Choi et al. 2010). The largest MW dextran included in the present study (500 kDa) showed no statistically significant increased fluorescence over baseline controls at any of the pressures studied. However, punctate intensity was seen in the brain at a pressure of 0.42 MPa. It is possible that at this pressure, FUS resulted in permeation of the endothelial cell membranes (sonoporation), which would allow movement of molecules into the endothelium, but not further into the brain parenchyma. A similar result came from a larger dextran (2000 kDa) studied by Choi et al. (Choi et al. 2010). Importantly, this sets a practical limit on the size of molecule that can be safely delivered with the FUS-mediated BBB opening methodology.

Notably, we have found that BBB opening using a pressure of 0.26 MPa may be sufficient for whole brain treatment in mice when employing smaller molecular weight agents (< 3 kDa). However, when using larger molecular weight compounds, e.g. monoclonal antibodies (70-155 kDa), multi-site BBB opening will likely be necessary to treat extended regions of the brain. The extravasation of molecules was also found to be dependent on FUS pressure. At the lowest pressures studied, small molecules (MRI contrast or 3 kD dextran) readily enter the brain, but the largest dextran molecules only extravasated at high ultrasound pressure. However, even at the highest FUS pressure used in this study to investigate dextran extravasation, 0.42 MPa, only minor damage was seen in the brain (Figure A1). Extravasation of large molecules may also be achievable at even lower ultrasound pressures because it seems that a threshold exists between 0.26 and 0.42 MPa. These conclusions are primarily drawn from qualitative analysis of the images (Figs. 2 and 3) and not the objective quantification (Figs. 4 and 5). For quantitative analysis, several regions of fluorescence were found to not be statistically different from control animals, particularly for low ultrasound pressure and large MW dextran.

The extent of BBB opening seen with the in vivo MRI and fluorescence imaging reflects both the opening of the BBB to the MRI contrast agents as well as diffusion of MRI contrast agent within the brain parenchyma. The diffusion coefficient of dextrans calculated in this work are highly dependent on molecular weight and are consistent with previous studies using optical imaging of dextran injected directly into rat cortex and turtle cerebellum

(Wolak and Thorne 2013; Xiao et al. 2008). The low diffusion coefficient of the 70 kDa dextran (0.157 $\mu m^2/s$) indicates that only the brain tissue in close proximity of the BBB opening would get exposed to molecules of this size. The even lower diffusion coefficient of the 500 kDa dextran (0.036 $\mu m^2/s$) indicates virtually no tissue outside the endothelial cell layer of the opening would get exposed to this size molecule. The diffusion coefficient of the 3 kDa dextran studied here is in the same order of magnitude, but higher than that measured in the previous studies. It is possible this difference is due to the different location in the brains studied, differences in the delivery technique (i.e. direct injection vs FUS-mediated BBB opening), but could also result from limitations in our diffusion model. By restricting the "sources" of dextran to the punctate spots seen in the images of the larger molecular weight dextran, the model does not account for the potential existence of smaller openings in the BBB at locations distant from puncta. Intensity arising from distant locations would be interpreted as an increase in the diffusion of dextran from the source (Figure A2).

Diffusion of molecules in the brain is dependent on many factors, including MW of the diffusing molecule as well as the geometry and tortuosity of the extracellular space. Estimates of volume fraction of extracellular space (ECS) in the brain are up to 20% and a ECS "width" of 38-64 nm (Syková and Nicholson 2008; Thorne and Nicholson 2006). Based on these measurements, diffusion of the 500 kDa dextran is expected to be severely restricted in the ECS of the brain, consistent with the results in Figs. 3-6. The smaller molecules showed significant diffusion at all ultrasound pressures, indicating that the ECS width does not inhibit diffusion at these molecular sizes. This is a very important consideration in translation of this FUS methodology to humans. With small molecular weight agents, e.g. traditional chemotherapeutics, it may be enough to open a localized region of the brain and allow the agent to diffusion into the parenchyma. However, larger MW agents, e.g. antibodies with MWs near 70 kDa, may require multiple sites of BBB opening to treat a selected region of brain tissue.

With the capability of delivering molecules to the brain parenchyma, it is also important to know the half-life of these molecules in the brain. While the molecules diffuse into the brain, they are also being cleared through various pathways using specific CSF generation and drainage sites (Ransohoff and Engelhardt 2012). Both diffusion and clearance can technically be modeled, but have complex multi-compartment kinetics that are difficult to characterize independently (Tarasoff-Conway et al. 2015). If a therapeutic is rapidly cleared by the CSF, it may require sustained infusion to have a therapeutic effect. Size plays a key role in the half-life for elimination in the brain. For a small molecule (<500 Da), this is usually less than 0.1 hour (Saltzman and Radomsky 1991) which is much more rapid than large molecules (90 hours for 70 kDa FITC-dextran) (Dang and Saltzman 1992).

For small molecules, rapid clearance from the CSF and unrestricted renal filtering suggests that a bolus IV injection of a therapeutic is not the best course of action when attempting to maximize delivery to the brain. Instead, a subcutaneous or intraperitoneal injection is preferable. Large molecules, however, are more likely to remain in the vasculature for days, but delivery to the brain suffers from a short amount of time that the BBB is open to these molecules. However, once in the brain, large molecules will persist in the brain for days (Dang and Saltzman 1992).

Clearance systems in the brain not only include the BBB, but also intracellular and extracellular degradation, CSF bulk flow (to the CSF sink, perivascular drainage and perivascular extracellular fluid), and CSF absorption (of the circulatory system, and the meningeal lymphatic vessels). Some clearance systems have multiple destinations, and each system has multiple factors that affect the clearance, such as sleep, ISF flow rate, age, genetics, and molecular interactions (Tarasoff-Conway et al. 2015). While it is important to understand how clearance mechanisms impact the fate of drugs in the brain, it is impractical to generate models for each mechanism to predict overall clearance rates. Instead, animal models can be used with model therapeutics or labeled therapeutics to model pharmacokinetic and biodistribution parameters.

There are other pharmacokinetics that could greatly impact the therapeutic effect of drugs delivered via MRgFUS. The half-life of drugs in the brain, plasma half-life, closure of the BBB over time, and molecular diffusion should all be considered. If a therapeutic agent is in the vasculature, and the BBB remains open, the brain will receive a continuous dose of therapeutic. However, BBB opening is transient and therefore closes over time (Marty et al. 2012). As it closes, fenestrations in the capillary endothelium become smaller and reduce the size threshold for molecules that can cross into the brain parenchyma. Marty et al. (Marty et al. 2012) utilized MR imaging with custom MR contrast agents of various sizes (1 to 65 nm) to model the half-closure time of the BBB. Half-closure time is defined as the time it takes for the BBB to close by half for a particular molecule size. The diameters of imaging agents used in the current study are listed in Table 2, along with estimated half-closure times. From these data, large molecules have a very short amount of time to extravasate, i.e. a short half-closure time, and should be injected before or immediately following BBB opening. Conversely, small molecules would benefit from having long circulation times in the vasculature in order to maximize dose to the brain. With a BBB half-closure time for 500 kDa at only 2 minutes, and a very low diffusion coefficient, there is essentially no time for significant amounts to extravasate into the brain parenchyma. These findings are consistent with previous studies that have shown 3 to 8 nm particles can cross the BBB 20 minutes after it has been opened, but not large molecules (Choi et al. 2010). The pressure and frequency used to determine these size limitations was 0.45 MPa at 1.5 MHz (MI = 0.37), which is below the inertial cavitation threshold that is necessary to deliver large molecules to the brain (Chen et al. 2013), and below the BBB opening threshold proposed by other studies (McDannold et al. 2008). This suggests that inertial cavitation causes the formation of pores that are inherently different than when stable cavitation is used to open the BBB. Inertial cavitation has been shown to cause more microvascular damage (Burgess and Hynynen 2014), indicating that pores are perhaps larger and/or more damaged and require more time to heal.

Conclusions

Contrast agents of various sizes, relevant to biological therapeutics, were simultaneously delivered to mouse brains using MRgFUS-mediated BBB opening and the distribution and diffusion of the molecules in the brain were determined using multispectral microscopy and molecular modeling. The volume of brain exposed to the molecules was inversely dependent on molecular weight at any given ultrasound pressure and increasing pressure resulted in

increased delivery in dextran up to 70 kDa. Diffusion coefficients within the brain were calculated indicating a strong inverse relationship between molecular weight and diffusion..

Supplementary Material

Refer to Web version on PubMed Central for supplementary material.

Acknowledgements

We would like to thank Dr. Marek Romanowski for assistance with the fluorescence microscopy experiments, and Drs. Russell Witte and Pier Ingram for their assistance with calibration of the FUS system. This work was supported by NIH grants R01-EB000343, T32-EB000809, Arizona Department of Health Services grant ADHS16-00005489 and the Arizona Alzheimer's Consortium.

Appendix:: Diffusion Model for Dextran in the Brain

The multispectral experiments carried out in this work ensure that the images from different molecular weight dextrans are inherently registered and can be directly and quantitatively compared. A mathematical model of diffusion was developed and applied to analyze the imaging data from three different size dextrans to characterize molecular diffusion within the brain.

Particles that can freely diffuse from a point source in three dimensional space will do so with a Gaussian or normal distribution (Nicholson et al. 2000) such that the concentration of the particle, C, at any distance from an origin, r, and time, t, can be calculated according to:

$$C = \frac{P}{\alpha}\frac{1}{(4D^{*}t\pi)^{3/2}}e^{\left(\frac{-r^{2}}{4D^{*}t}\right)} \quad \text{Eq. A.1}$$

where P is the moles of a substance deposited at the origin ($r = 0$) at time $t = 0$, and α is the fraction of the volume available for the particles to move in. D* is the effective diffusion coefficient of the particle, which is influenced by the size of the particle, the tortuosity of the brains extracellular space (ECS) and the matrix components within it. For diffusion of particles from a constant source, Equation A.1 is modified to

$$C = \frac{Q}{4\pi D^{*}r\alpha}\left(erfc\left(\frac{r}{2\sqrt{D^{*}t}}\right)\right) for\, t \leq \mathrm{d} \quad \text{Eq. A.2}$$

where Q is the constant release rate of particles at the source in moles per second, *erfc* is the complementary error function, t is time since initial release, and d is the period in which particles are being released. In applying these equations to our model, we assume that the concentration of dextran in the blood remains constant during the time that the BBB is open, and the BBB is opened at point sources which are allowing dextran to leak from the vasculature at a constant, but unknown rate. In our experiments, $t = d = 1200$ s (20 minutes, the amount of time allowed for the agent to circulate and diffuse into the brain) and Eq. A.2 can be simplified to

$$C = c_o\left(erfc\left(\frac{r}{2\sqrt{D^*(1200\,sec)}}\right)\right) \quad \text{Eq. A.3}$$

where the first term in the equation has been changed to c_o and represents the initial concentration of the particle at each point source.

Software for fitting images to Equation A.3 was written in MATLAB (Mathworks, Natick, MA) and outlined in Figure A1. Three fluorescence images of a single section (blue, red and green, corresponding to 3, 70 and 500 kDa dextran, respectively) are read into MATLAB. Raw images are thresholded to three standard deviations above the mean background on the side of the brain contralateral to BBB opening to remove autofluorescence. The local maxima in the green channel image are used to define the location of point sources for fluorescent molecules.

Visual inspection ensured that the centers of the punctate regions are colocalized with the local maxima. Local maxima pixels were returned to their original thresholded pixel values and served as the location for point sources in the model. A set of 2D convolution kernels were generated based on the diffusion model (Eq. A.3), such that $c_o = 1$, r is the distance from the point source. Kernels were generated for possible effective diffusion coefficient (D*) values from 0.0010 to 50 $\mu m^2/s$. The following set of possible D* values, each with 2 significant figures, were used to generate individual images: D* = {0.0010, 0.0020, … 0.099} … {0.10, 0.11, 0.12, … 0.99} … {1.0, 1.1, 1.2, … 9.9} … {10, 11, 12, … 50} µm2/s.

Each kernel was convolved with the local maxima image to generate a set of simulated fluorescence distributions, where each simulated image corresponds to a different value of D*. The simulated diffusion image that most closely matched the experimental fluorescence image is expected to have a D* that represents the fluorescent image, based on the r-squared (R^2) goodness-of-fit between the experimental and simulated image. The simulated diffusion images that produced the maximum R^2 value for the fluorescence image with which they were fitted, provided the estimate for D*. An example of the resulting best-fit images for a set of fluorescent images from a single slice are shown in Figure A2. The images produced from the diffusion model correlate well with respect to diffuse fluorescence signal, but does not replicate all of the punctate patterns seen in the raw images, particularly in the images of 3 kDa dextran.

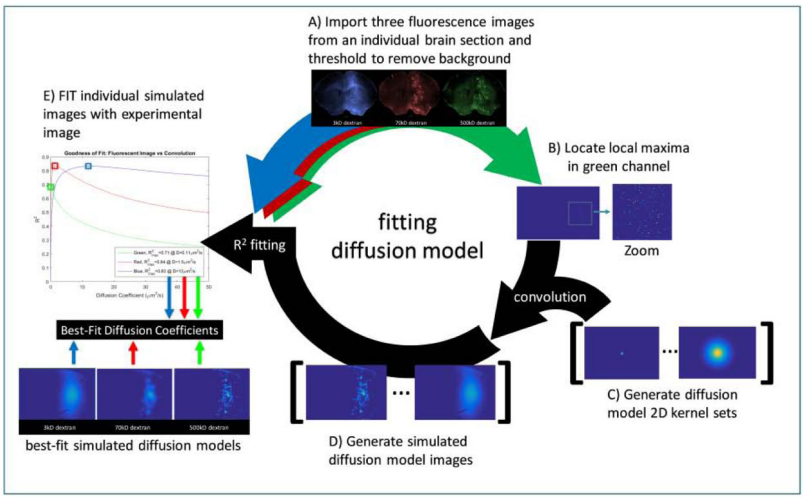

Figure A1.

Schematic of the diffusion model to determine effective diffusion coefficients, D*, of fluorescently labeled dextrans. A) A set of fluorescent images with molecules of various molecular weights and with spatially and temporally-matched BBB opening (blue, red, green images, top) was read into MATLAB. Raw images were thresholded to three standard deviations above the mean background. B) Local maxima representing the center of each punctuation in the 500 kDa fluorescence region were located. C) A set of 2D convolution kernels were generated based on the diffusion model (Eq. A.3) for a wide range of effective diffusion coefficient, D*, values. D) The images of local maxima generated in (B) were convolved with the set of kernels to generate a set of simulated fluorescence distributions. E) Each simulated distribution map and individual fluorescent images, for 3, 70 and 500 kDa dextran, were fit with a linear least squares. The coefficient of variation, R^2, for the regression was plotted versus the effective diffusion coefficient used to produce the simulated distribution. The D* value at the maximum R^2 was selected as the best fit diffusion coefficient.

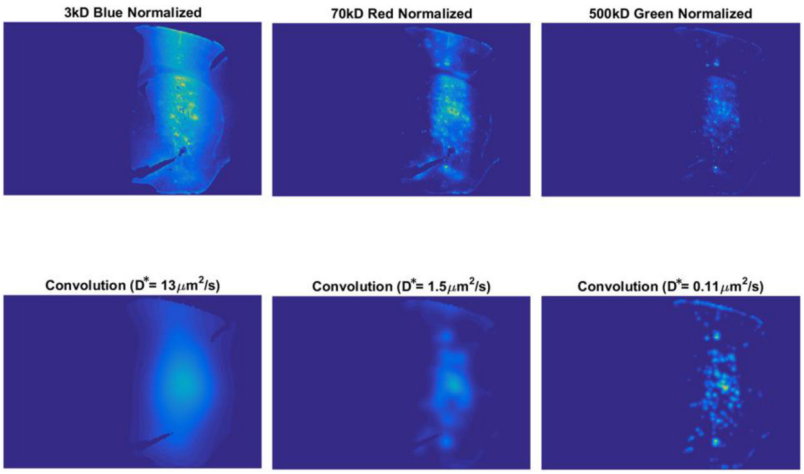

Figure A2.

Experimental (top row) and corresponding simulated (bottom row) fluorescence images for three different molecular weight dextrans (3, 70 and 500 kDa). Images were thresholded to reduce autofluorescence and are displayed using the same blue-yellow colormap for clarity of comparison. Best-fit simulated images were with diffusion modeling as described in the Appendix.

References

Baseri B, Choi JJ, Tung Y-S, Konofagou EE. Multi-Modality Safety Assessment of Blood-Brain Barrier Opening Using Focused Ultrasound and Definity Microbubbles: A Short-Term Study. Ultrasound Med Biol 2010;36.

Boado RJ, Hui EK-W, Lu JZ, Pardridge WM. Drug targeting of erythropoietin across the primate blood-brain barrier with an IgG molecular Trojan horse. J Pharmacol Exp Ther 2010;333:961–9. [PubMed: 20233799]

Burgess A, Dubey S, Yeung S, Hough O, Eterman N, Aubert I, Hynynen K. Alzheimer Disease in a Mouse Model: MR Imaging–guided Focused Ultrasound Targeted to the Hippocampus Opens the Blood-Brain Barrier and Improves Pathologic Abnormalities and Behavior. Radiology 2014;273:736–745. [PubMed: 25222068]

Burgess A, Hynynen K. Drug delivery across the blood-brain barrier using focused ultrasound. Expert Opin Drug Deliv 2014;11:711–21. [PubMed: 24650132]

Calias P, Banks WA, Begley D, Scarpa M, Dickson P. Intrathecal delivery of protein therapeutics to the brain: A critical reassessment. Pharmacol Ther 2014;144:114–122. [PubMed: 24854599]

Chen H, Konofagou EE. The Size of Blood–Brain Barrier Opening Induced by Focused Ultrasound is Dictated by the Acoustic Pressure. J Cereb Blood Flow Metab 2014;34:1197–1204. [PubMed: 24780905]

Chen H, Srivastava A, Sun T, Olumolade O, Konofagou EE. Delivery of different-size molecules by ultrasound-induced blood-brain barrier opening and its correlation with acoustic emission. J Acoust Soc Am 2013;134:4181–4181.

Choi JJ, Pernot M, Brown TR, Small SA, Konofagou EE. Spatio-temporal analysis of molecular delivery through the blood–brain barrier using focused ultrasound. Phys Med Biol 2007;52:5509–5530. [PubMed: 17804879]

Choi JJ, Wang S, Tung Y-S, Morrison B, Konofagou EE. Molecules of Various Pharmacologically-Relevant Sizes Can Cross the Ultrasound-Induced Blood-Brain Barrier Opening in vivo. Ultrasound Med Biol 2010;36:58–67. [PubMed: 19900750]

Chu P-C, Chai W-Y, Tsai C-H, Kang S-T, Yeh C-K, Liu H-L. Focused Ultrasound-Induced Blood-Brain Barrier Opening: Association with Mechanical Index and Cavitation Index Analyzed by

Dynamic Contrast-Enhanced Magnetic-Resonance Imaging. Sci Rep 2016;6:33264. [PubMed: 27630037]

Dang W, Saltzman WM. Dextran Retention in the Rat Brain Following Release from a Polymer Implant. Biotechnol Prog 1992;8:527–532. [PubMed: 1282018]

Downs ME, Buch A, Sierra C, Karakatsani ME, Chen S, Konofagou EE, Ferrera VP. Long-Term Safety of Repeated Blood-Brain Barrier Opening via Focused Ultrasound with Microbubbles in Non-Human Primates Performing a Cognitive Task Liebner S, ed. PLoS One 2015;10:e0125911. [PubMed: 25945493]

Gabathuler R. Approaches to transport therapeutic drugs across the blood–brain barrier to treat brain diseases. Neurobiol Dis 2010;37:48–57. [PubMed: 19664710]

Gage GJ, Kipke DR, Shain W. Whole animal perfusion fixation for rodents. J Vis Exp 2012; 65:e3564

Harpel K, Baker RD, Amirsolaimani B, Mehravar S, Vagner J, Matsunaga TO, Banerjee B, Kieu K. Imaging of targeted lipid microbubbles to detect cancer cells using third harmonic generation microscopy. Biomed Opt Express 2016;7:2849. [PubMed: 27446711]

Howles GP, Bing KF, Qi Y, Rosenzweig SJ, Nightingale KR, Johnson GA. Contrast-enhanced in vivo magnetic resonance microscopy of the mouse brain enabled by noninvasive opening of the blood-brain barrier with ultrasound. Magn Reson Med 2010;64:995–1004. [PubMed: 20740666]

Hynynen K, McDannold N, Sheikov N, Jolesz F, Vykhodtseva N. Local and reversible blood-brain barrier disruption by noninvasive focused ultrasound at frequencies suitable for trans-skull sonications. Neuroimage 2005;24.

Hynynen K, McDannold N, Vykhodtseva N, Jolesz F. Noninvasive MR imaging-guided focal opening of the blood-brain barrier in rabbits. Radiology 2001;220.

Hynynen K, McDannold N, Vykhodtseva N, Jolesz FA. Non-invasive opening of BBB by focused ultrasound. Brain Edema XII 2003 pp. 555–558.

Jordão JF, Ayala-Grosso CA, Markham K, Huang Y, Chopra R, McLaurin J, Hynynen K, Aubert I. Antibodies Targeted to the Brain with Image-Guided Focused Ultrasound Reduces Amyloid-β Plaque Load in the TgCRND8 Mouse Model of Alzheimer's Disease El Khoury J, ed. PLoS One 2010;5:e10549. [PubMed: 20485502]

Kinoshita M, McDannold N, Jolesz F, Hynynen K. Targeted delivery of antibodies through the blood-brain barrier by MRI-guided focused ultrasound. Biochem Biophys Res Commun 2006a;340.

Kinoshita M, McDannold N, Jolesz F, Hynynen K. Noninvasive localized delivery of Herceptin to the mouse brain by MRI-guided focused ultrasound-induced blood-brain barrier disruption. Proc Natl Acad Sci U S A 2006b;103.

Liang Z, Liu X, Zhang N. Dynamic resting state functional connectivity in awake and anesthetized rodents. Neuroimage 2015;104:89–99. [PubMed: 25315787]

Lipsman N, Meng Y, Bethune AJ, Huang Y, Lam B, Masellis M, Herrmann N, Heyn C, Aubert I, Boutet A, Smith GS, Hynynen K, Black SE. Blood–brain barrier opening in Alzheimer's disease using MR-guided focused ultrasound. Nat Commun 2018;9:2336. [PubMed: 30046032]

Marquet F, Teichert T, Ferrera V, Konofagou EE. Feasibility of noninvasive cavitation-guided blood-brain barrier opening using focused ultrasound and microbubbles in nonhuman primates. Appl Phys Lett 2011a;98:163704. [PubMed: 21580802]

Marquet F, Tung Y-S, Teichert T, Ferrera VP, Konofagou EE. Noninvasive, Transient and Selective Blood-Brain Barrier Opening in Non-Human Primates In Vivo Brechbiel MW, ed. PLoS One 2011b;6:e22598. [PubMed: 21799913]

Marty B, Larrat B, Van Landeghem M, Robic C, Robert P, Port M, Le Bihan D, Pernot M, Tanter M, Lethimonnier F, Mériaux S. Dynamic Study of Blood–Brain Barrier Closure after its Disruption using Ultrasound: A Quantitative Analysis. J Cereb Blood Flow Metab 2012;32:1948–1958. [PubMed: 22805875]

McDannold N, Vykhodtseva N, Hynynen K. Targeted disruption of the blood–brain barrier with focused ultrasound: association with cavitation activity. Phys Med Biol 2006;51:793–807. [PubMed: 16467579]

McDannold N, Vykhodtseva N, Hynynen K. Effects of Acoustic Parameters and Ultrasound Contrast Agent Dose on Focused-Ultrasound Induced Blood-Brain Barrier Disruption. Ultrasound Med Biol 2008;34:930–937. [PubMed: 18294757]

Nhan T, Burgess A, Cho EE, Stefanovic B, Lilge L, Hynynen K. Drug delivery to the brain by focused ultrasound induced blood–brain barrier disruption: Quantitative evaluation of enhanced permeability of cerebral vasculature using two-photon microscopy. J Control Release 2013;172:274–280. [PubMed: 24008151]

Nicholson C, Chen KC, Hrabětová S, Tao L. Diffusion of molecules in brain extracellular space: Theory and experiment. Prog Brain Res 2000;125:129–154. [PubMed: 11098654]

O'Reilly MA, Hynynen K. Blood-brain barrier: real-time feedback-controlled focused ultrasound disruption by using an acoustic emissions-based controller. Radiology 2012;263:96–106. [PubMed: 22332065]

Pardridge WM. The blood-brain barrier: Bottleneck in brain drug development. NeuroRX 2005;2:3–14. [PubMed: 15717053]

Pardridge WM. Drug transport in brain via the cerebrospinal fluid. Fluids Barriers CNS 2011;8:7. [PubMed: 21349155]

Ransohoff RM, Engelhardt B. The anatomical and cellular basis of immune surveillance in the central nervous system. Nat Rev Immunol 2012;12:623–635. [PubMed: 22903150]

Raymond SB, Treat LH, Dewey JD, McDannold NJ, Hynynen K, Bacskai BJ. Ultrasound Enhanced Delivery of Molecular Imaging and Therapeutic Agents in Alzheimer's Disease Mouse Models Bush AI, ed. PLoS One 2008;3:e2175. [PubMed: 18478109]

Saltzman WM, Radomsky ML. Drugs released from polymers: diffusion and elimination in brain tissue. Chem Eng Sci 1991;46:2429–2444.

Samiotaki G, Vlachos F, Tung Y-S, Konofagou EE. A quantitative pressure and microbubble-size dependence study of focused ultrasound-induced blood-brain barrier opening reversibility in vivo using MRI. Magn Reson Med 2012;67:769–777. [PubMed: 21858862]

Sun T, Samiotaki G, Wang S, Acosta C, Chen CC, Konofagou EE. Acoustic cavitation-based monitoring of the reversibility and permeability of ultrasound-induced blood-brain barrier opening. Phys Med Biol 2015;60:9079–9094. [PubMed: 26562661]

Syková E, Nicholson C. Diffusion in brain extracellular space. Physiol Rev 2008;88:1277–340. [PubMed: 18923183]

Tarasoff-Conway JM, Carare RO, Osorio RS, Glodzik L, Butler T, Fieremans E, Axel L, Rusinek H, Nicholson C, Zlokovic BV, Frangione B, Blennow K, Ménard J, Zetterberg H, Wisniewski T, de Leon MJ. Clearance systems in the brain-implications for Alzheimer disease. Nat Rev Neurol 2015;11:457–70. [PubMed: 26195256]

Thorne RG, Nicholson C. In vivo diffusion analysis with quantum dots and dextrans predicts the width of brain extracellular space. Proc Natl Acad Sci 2006;103:5567–72. [PubMed: 16567637]

Tung Y-S, Vlachos F, Choi JJ, Deffieux T, Selert K, Konofagou EE. *In vivo* transcranial cavitation threshold detection during ultrasound-induced blood–brain barrier opening in mice. Phys Med Biol 2010;55:6141–6155. [PubMed: 20876972]

Wolak DJ, Thorne RG. Diffusion of Macromolecules in the Brain: Implications for Drug Delivery. Mol Pharm 2013;10:1492–1504. [PubMed: 23298378]

Xiao F, Nicholson C, Hrabe J, Hrabětová S. Diffusion of Flexible Random-Coil Dextran Polymers Measured in Anisotropic Brain Extracellular Space by Integrative Optical Imaging. Biophys J 2008;95:1382–1392. [PubMed: 18456831]

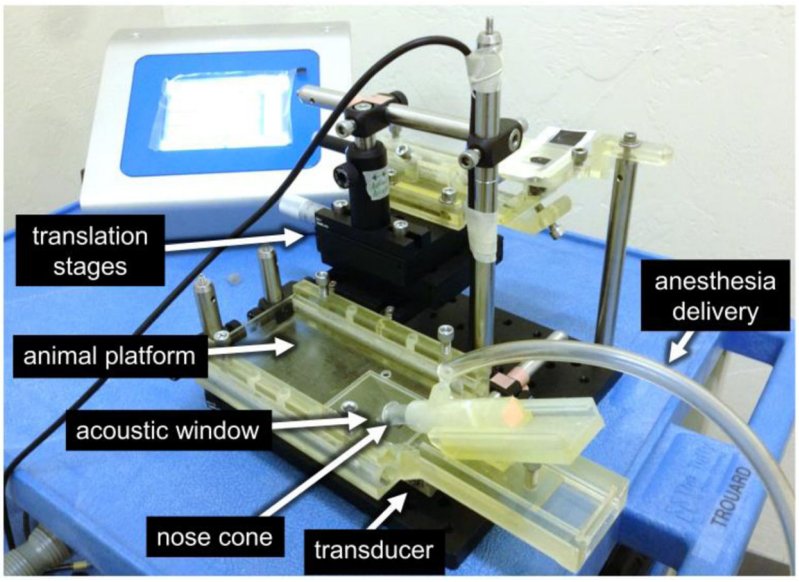

Figure 1.

Benchtop FUS apparatus for BBB opening in mice. The 22 mm diameter single element transducer sits directly beneath an animal platform that supports a mouse in the supine position while allowing ultrasound to be applied into the mouse brain. The apparatus consisted of custom made 3D-printed parts (light yellow objects) and commercial optomechanical components.

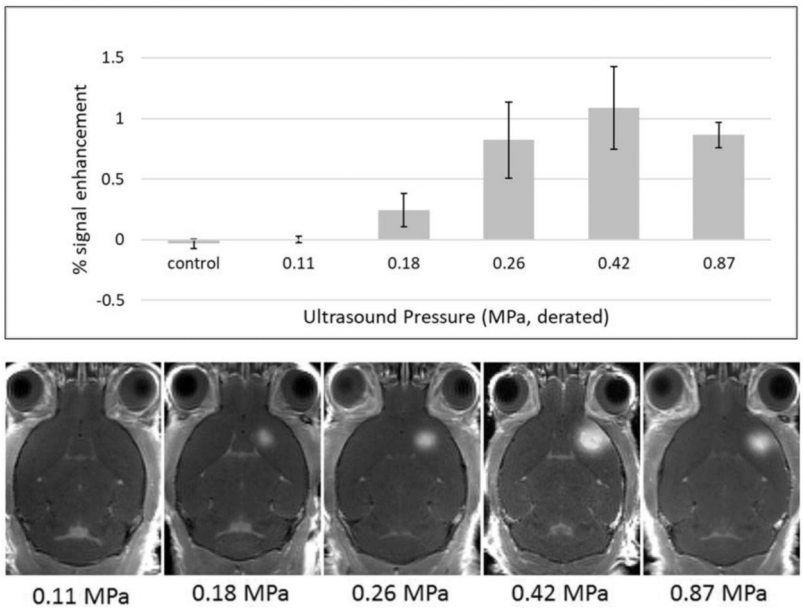

Figure 2.

Evaluation of BBB opening with various FUS pressures in mice. Top: Bar chart showing percent MRI signal enhancement in the brain for different FUS pressures used to open the BBB. Error bars represent standard error of the mean values. Bottom: Representative transverse MR images obtained after BBB opening using different FUS pressures.

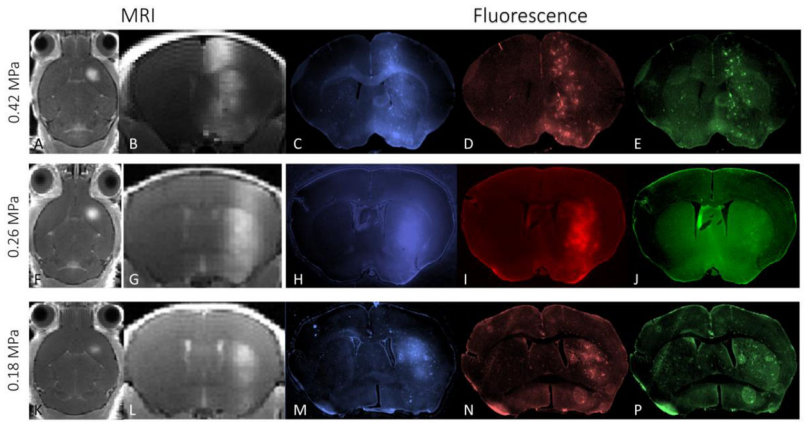

Figure 3.

Transverse and coronal MRI and fluorescence images of representative mice that received FUS-mediated BBB opening. Three different FUS pressures were used (0.42, 0.26, 0.18 MPa, top to bottom row, respectively). The T1-weighted MR images (grayscale on left) shows signal enhancement from the presence of MRI contrast agent on the right side of the brain. The fluorescence images (in color, on right) show signal arising from 3, 70 and 500 kDa dextran injected IV and allowed to circulate for 20 minutes prior to in vivo perfusion.

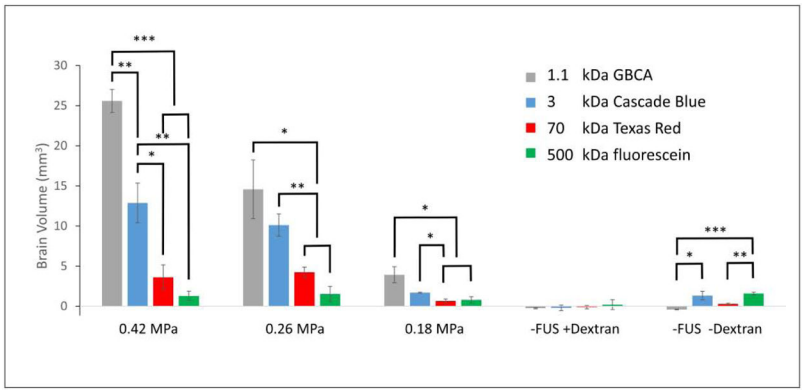

Figure 4.

Brain volume accessed by different molecular weight agents at different levels of focused ultrasound pressure, categorically sorted by ultrasound pressure. Bar heights represent mean volume of brain containing the imaging agents. Error bars represent ±SEM (standard error of the mean). Statistical significance is displayed with asterisks (* = $p < 0.05$, ** = $p < 0.01$, *** = $p < 0.001$), and were calculated only for successively-sized imaging agents. Non-zero values in the control sections (−FUS +Dextran and −FUS −Dextran) arise from autofluorescence of the tissue and fixative.

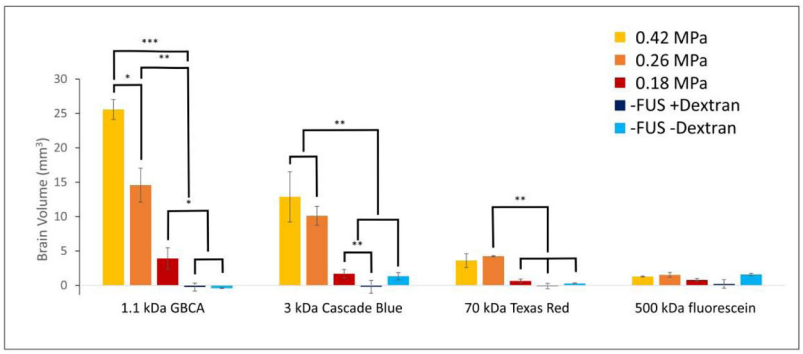

Figure 5.

Brain volume accessed by different molecular weight agents at different levels of focused ultrasound pressure, categorically sorted by imaging agent. Bar heights represent mean volume of brain containing imaging agents. Error bars represent ±SEM (standard error of the mean). Statistical significance is displayed with asterisks (*p < 0.05, **p < 0.01, ***p < 0.001), and were calculated to determine difference in brain volume due to pressure. Non-zero values in the control sections (−FUS +Dextran and −FUS −Dextran) arise from autofluorescence of the tissue and fixative.

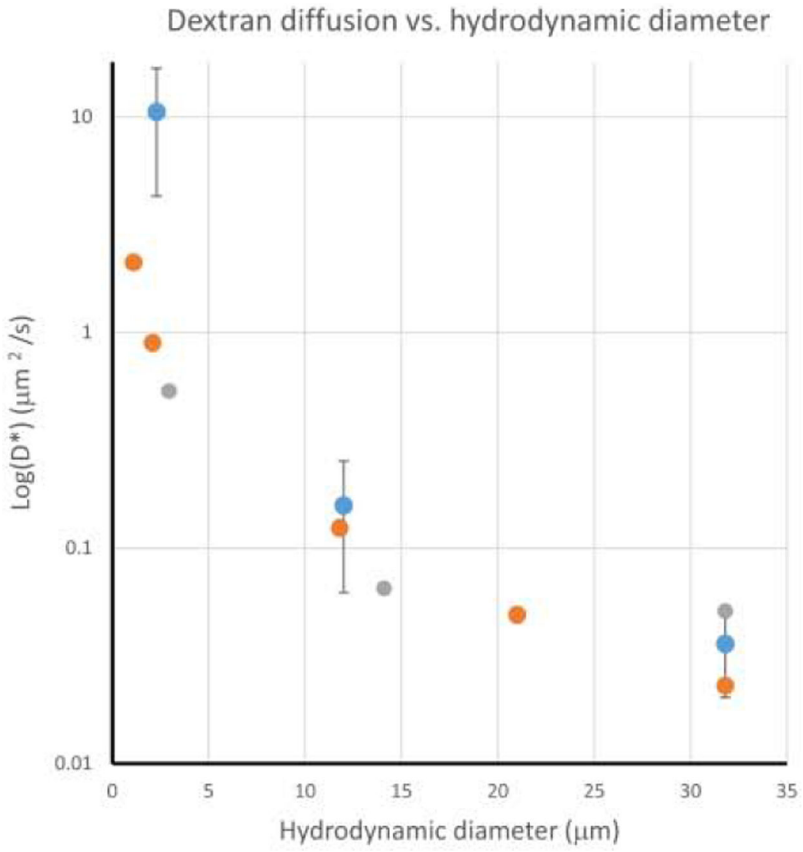

Figure 6.

Effective diffusion coefficients, D*, of dextran molecules in the brain versus hydrodynamic diameter, d_H. Values are plotted on a Log scale to assist comparison. Values from the present study (blue dots) are from one section per mouse (n=4) using 0.42 MPa FUS. Effective diffusion coefficients of macromolecules measured in vivo rat cortex (gray dots) (Wolak and Thorne 2013) and ex vivo turtle cerebellum (orange dots) (Liang et al. 2015) are included for reference.

Table 1.

Molecular weight and fluorescence properties of dextran molecules.

Dextran MW (kDa)	Fluorescent Moiety (name)	Absorption/emission maximum (nm)	Emission “color”
3	Cascade Blue	400/420	Blue
70	Texas Red	595/615	Red
500	Fluorescein	494/518	Green

Table 2.

Characteristics of molecular diameter and blood brain barrier half-closure times for contrast agents used in this study (Marty et al. 2012).

Molecule	Molecular Diameter (nm)	Half-Closure Time (hrs)
Gd-BOPTA	0.82	5.7
3 kDa Dextran	2.3	3.1
70 kDa Dextran	10.2	0.28
500 kDa Dextran	30.6	0.033